Biosensors and Bioelectronics 153 (2020) 112019

Contents lists available at ScienceDirect

Biosensors and Bioelectronics

journal homepage: http://www.elsevier.com/locate/bios

3D bimetallic Au/Pt nanoflowers decorated needle-type microelectrode for direct *in situ* monitoring of ATP secreted from living cells

Qin Zhu [a], Bo Liang [a,**], Yitao Liang [a], Lin Ji [b], Yu Cai [a], Ke Wu [b], Tingting Tu [a], Hangxu Ren [a], Bobo Huang [a], Jinwei Wei [a], Lu Fang [c], Xiao Liang [b], Xuesong Ye [a,*]

[a] *Biosensor National Special Laboratory, Key Laboratory of Biomedical Engineering of Ministry of Education, College of Biomedical Engineering and Instrument Science, Innovation Center for Minimally Invasive Technique and Device, Zhejiang University, Hangzhou, 310027, PR China*

[b] *Key Laboratory of Laparoscopic Technology of Zhejiang Province, Department of General Surgery, Sir Run-Run Shaw Hospital, School of Medicine, Zhejiang University, Hangzhou, 310016, PR China*

[c] *College of Automation, Hangzhou Dianzi University, Hangzhou, 310018, PR China*

ARTICLE INFO

Keywords:
ATP microelectrode biosensor
3D bimetallic nanoflowers
Long-term stability
In situ ATP monitoring
PC12 cells

ABSTRACT

Adenosine triphosphate (ATP) plays a crucial role in energy metabolism and extracellular purinergic signaling. A 3D bimetallic Au/Pt nanoflowers decorated ATP microelectrode biosensor prepared by facile and effective template-free electrodeposition was firstly reported, realizing local detection of cellular ATP secretion. The ATP biosensor was developed by co-immobilization of glucose oxidase and hexokinase, exhibiting long-term stability (79.39 ± 9.15% of its initial value remained after 14 days at 4 °C) and high selectivity with a limit of detection down to 2.5 μM (S/N = 3). The resulting ATP biosensor was then used for direct *in situ* monitoring of ATP secreted from living cells (PC12) with the stimulation of high K^+ solutions. The obtained current was about 21.6 ± 3.4 nA (N = 6), corresponding to 12.2 ± 2.8 μM ATP released from cells, right in the micromolar range and consistent with the suggested levels. The 3D bimetallic Au/Pt nanoflowers possess excellent catalytic activity and large electroactive surface area, contributing to enzymatic activity preservation and long-term stability. This work provides a promising platform for long-time monitoring of other neurotransmitters and secretions in cellular glycolysis and apoptosis processes in the future.

1. Introduction

Adenosine triphosphate (ATP) serves as the high-energy compound in living organisms (Deng et al., 2017; Robinson et al., 2008), plays a crucial role in extracellular purinergic signaling (Morciano et al., 2017; Burnstock, 2007; Evans et al., 1992; Gourine et al., 2005) and has noted effects on cell growth, proliferation and death (Hecht et al., 2013; Qian et al., 2016). Besides resulting from cell death, ATP is now generally verified to be secreted via nonlytic release which is possibly the main mechanism (Morciano et al., 2017; Patergnani et al., 2014; Zhang et al., 2007). The modulation of purine release and sensing during diseases may provide promising therapeutic insights for sterile liver injury (Oliveira et al., 2013). It is believed that direct *in situ* monitoring of ATP secreted from living cells will shed light on the mechanism study of purinergic signaling.

While various techniques have been developed for ATP measurements, some problems still remain to be addressed. For example, conventional bioluminescent luciferin-luciferase assay can only obtain ATP concentration in bulk solution and usually diluted ATP levels are detected (Beigi et al., 1999; Yang et al., 2002). Commercial kits can offer convenient assays for detection but it is hard to realize real-time monitoring. Although aptamer ATP biosensor can identify ATP at a low concentration, the complementary strand of the aptamer is difficult to recycle after being released (Ma et al., 2019; Yao et al., 2009). Amperometric ATP microelectrode biosensors based on glucose oxidase (GOx) and hexokinase (HEX) feature high sensitivity, rapid response and continuous monitoring with adequate spatial and temporal resolution and have been successfully adopted for *in vitro* or *in vivo* applications (Hecht et al., 2013; Zhang et al., 2016; Ziller et al., 2017). Despite this method could achieve *in situ* monitoring, long-term stability was not satisfactory as reported (Kucherenko et al., 2014; Patel et al., 2011; Ziller et al., 2017). In fact, long-term stability is of vital

* Corresponding author.
** Corresponding author.
E-mail addresses: boliang1986@zju.edu.cn (B. Liang), yexuesong@zju.edu.cn (X. Ye).

https://doi.org/10.1016/j.bios.2020.112019
Received 23 November 2019; Received in revised form 6 January 2020; Accepted 11 January 2020
Available online 11 January 2020

significance for biosensors, especially for real-time continuous monitoring of cellular metabolites during cell differential, proliferation, motility and death (Burnstock, 2016).

The long-term stability was mainly related to the activity preservation of enzyme immobilized, which becomes a key issue because direct contact of enzymes with bare electrode surface causes the conformational changes in enzyme structure and the loss of enzymatic activity (Secundo, 2013). However, most researches about amperometric ATP biosensors focus on polymer modification to immobilize enzyme (Hecht et al., 2013; Patel et al., 2011; Ziller et al., 2017) and there is rare work on nanostructure modification to maintain enzyme activity by increasing electroactive surface area.

Bimetallic nanoflowers have attracted much attention for ultrasensitive detection of biomolecules (Tang et al., 2018) and cancer biomarkers (Liu et al., 2017), owing to the improved catalytic activity caused by the synergic effect (Chen et al., 2018; Gilroy et al., 2016) and large surface area and enhanced number of active sites derived from nanoflower-like morphology (Liu et al., 2017; Wang et al., 2018). Template-free electrodeposition (Guo et al., 2012; Taurino et al., 2015) is preferred compared to chemical synthesis method (D. et al., 2018; Yang et al., 2018), due to its simplicity, reproducibility, more intact and controllable morphology for follow-up biomolecule modification. However, reports on bimetallic Au/Pt nanoflowers developed by template-free electrodeposition to maintain enzyme activity are rare, the morphology and performance are not satisfactory and their application for ATP determination has not been explored thus far.

Here we firstly present a 3D bimetallic Au/Pt nanoflowers decorated ATP biosensor prepared by facile and effective template-free electrodeposition and realize local detection of cellular ATP secretion. Considering conventional microelectrode package techniques are very complicated (Russell et al., 2019), we also firstly proposed a simple fabrication protocol to obtain needle-types microelectrodes, as shown in Scheme 1. 3D bimetallic Au/Pt nanoflowers eventually formed a layer-by-layer nanostructure: the Au spikes as the base layer with non-uniform current distribution and enhanced conductivity; the Pt nanoflowers as the catalytic layer with large surface area and numerous active sites. Then a dual enzyme ATP biosensor was developed by the co-immobilization of GOx and HEX with glutaraldehyde cross-linking and exhibited a low limit of detection, long-term stability, high selectivity and satisfactory sensitivity. The proposed ATP biosensor was applied for direct *in situ* monitoring of ATP secreted from living cells. Several contrast tests were conducted to ensure the validity. The change of ATP levels induced by the stimulation of high K^+ solutions was identified successfully and in consistent with the suggested levels.

2. Experimental

2.1. Simple fabrication of needle-type microelectrode

Apparatus and reagents are listed in Supporting Information. Stainless-steel acupuncture microneedles were polished by 3000 grit abrasive papers with 80 mg/mL Alumina dispersion (0.05 μm), followed by sonication in ethanol and deionized ultrafiltered water. Then the stainless-steel acupuncture microneedle (160 μm in diameter) was inserted into the outlet of a hot melt glue gun and then pulled out. Hot melt glue wrapped the microneedle totally and solidified very quickly in the air. Then a surgical blade was used to cut off the glue under a microscope and then a length of 1 mm of the microneedle was exposed at the tip. To ensure the insulation of the glue after cutting, the electrode was put close to a soldering iron for several seconds. In the end, the microneedle tip was used as a needle-type microelectrode (160 μm in diameter, 1 mm in length). The detailed fabrication process for needle-type microelectrode is demonstrated in Scheme 1.

2.2. Electrochemical synthesis of 3D bimetallic Au/Pt nanoflowers

The electrode was immersed in 1 M H_2SO_4 solution and treated by Cyclic voltammetry (CV) with potential window from −0.4 to 0.6 V at a scan rate of 100 mV/s for 25 cycles, then rinsed with deionized ultrafiltered water. The electrode was then immersed in 10 mmol dm^{-3} $HAuCl_4$/0.5 mol dm^{-3} HCl solution with an applied potential of 0 V for 300 s. After rinsing with deionized ultra-filtered water and dried in the air, the electrodes were immersed in 10 mmol dm^{-3} H_2PtCl_6/0.1 mol dm^{-3} HCl solution with an applied potential of −0.3 V for 450 s. Different concentration of $HAuCl_4$ solution and growth time for Au spikes were applied for the optimization of Pt nanoflowers. Chronoamperometry experiments were carried out in 0.01 M PBS with successive injections of hydrogen peroxide to explore the catalytic performance. Cyclic voltammetry of 10 mM $[Fe(CN)_6]^{3-/4-}$ in 0.1 M KCl solution with scan rate of 50 mV/s and electrochemical impedance spectroscopy (EIS) with a frequency ranging from 0.1 Hz to 1 M Hz in 5 mM $[Fe(CN)_6]^{3-/4-}$ containing 0.1 M KCl have also been performed.

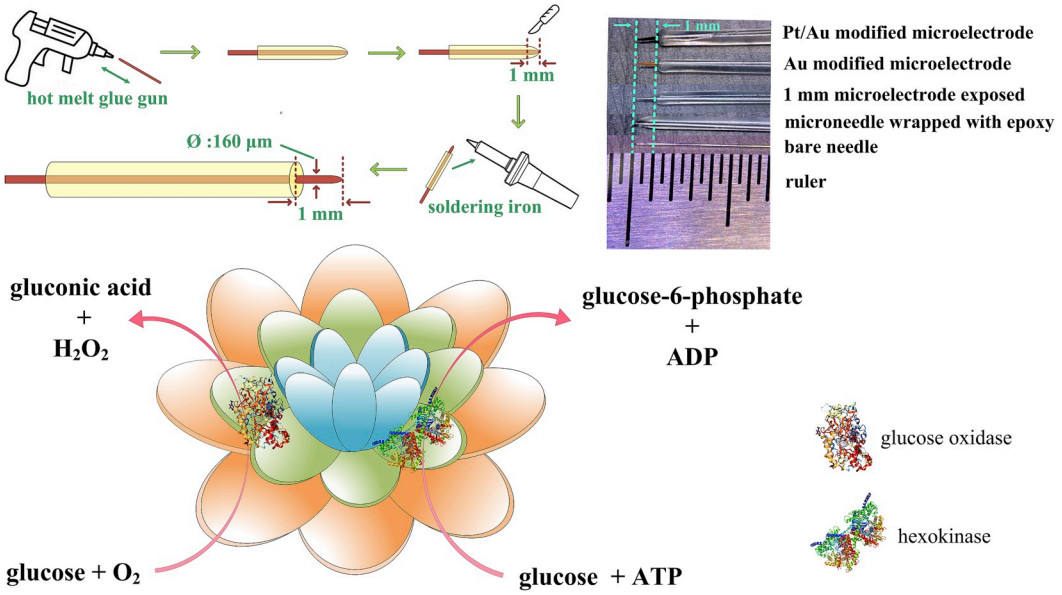

Scheme 1. Schematic illustration of needle-type microelectrode fabrication and the determination mechanism of ATP biosensor based on bimetallic Au/Pt nanoflowers.

2.3. Fabrication of ATP biosensor

To immobilize enzyme, the electrode was dipped into an enzyme solution for 3 h and stored at 4 °C. The enzyme solution containing 2 mg/mL glucose oxidase, 8 mg/mL hexokinase, 6 mg/mL BSA and 1 μL glycerin was prepared in 1 mL PBS. After dried at 4 °C for 20 min, the enzyme was cross-linked by glutaraldehyde (25%) at 37 °C for 20 min. The sensitivity of ATP biosensor was tested at an applied potential of 0.6 V in 0.01 M PBS (18 mM Mg^{2+}, pH = 6.0) unless declared specifically.

2.4. Cell culture

The highly-differentiated rat adrenal pheochromocytoma (PC12) cells were cultured in GNM31800 RPMI 1640 culture medium supplemented with 10% fetal bovine serum (FBS) and 1% penicillin-streptomycin (PS) at pH 7.4 in cell culture dishes (Corning, 35 mm × 10 mm, 430165). Cells were cultured at 37 °C in a humidified atmosphere (5% CO_2) for 2 days to form a monolayer.

2.5. In situ determination of cellular ATP release

For *in situ* determination of ATP released by PC12 cells, GNM31800 RPMI 1640 culture medium was exchanged with phosphate-buffered saline (PBS) containing 3 mM glucose and 18 mM magnesium. In order to ensure that the current drop was not induced by the decrease in the concentration of local glucose, stimulation solutions were prepared based on the above solution.

After *z*-positioning of the three-electrode system with the micromanipulator, the working electrode was biased at +0.60 V *vs.* Ag/AgCl. After achieving a stable baseline, 2.5 μL 0.1 M K^{+} stimulation solution was added to stimulate PC12 cells to release ATP. For comparison, a cell culture dish without PC12 cells was also detected. To ensure that the ATP biosensor was still effective after detection, external ATP stimulation solution was added afterwards in both experiments.

3. Results and discussion

3.1. Characterization of 3D bimetallic Au/Pt nanoflowers

Hot glue adhesive is introduced for insulation and there is no gold or

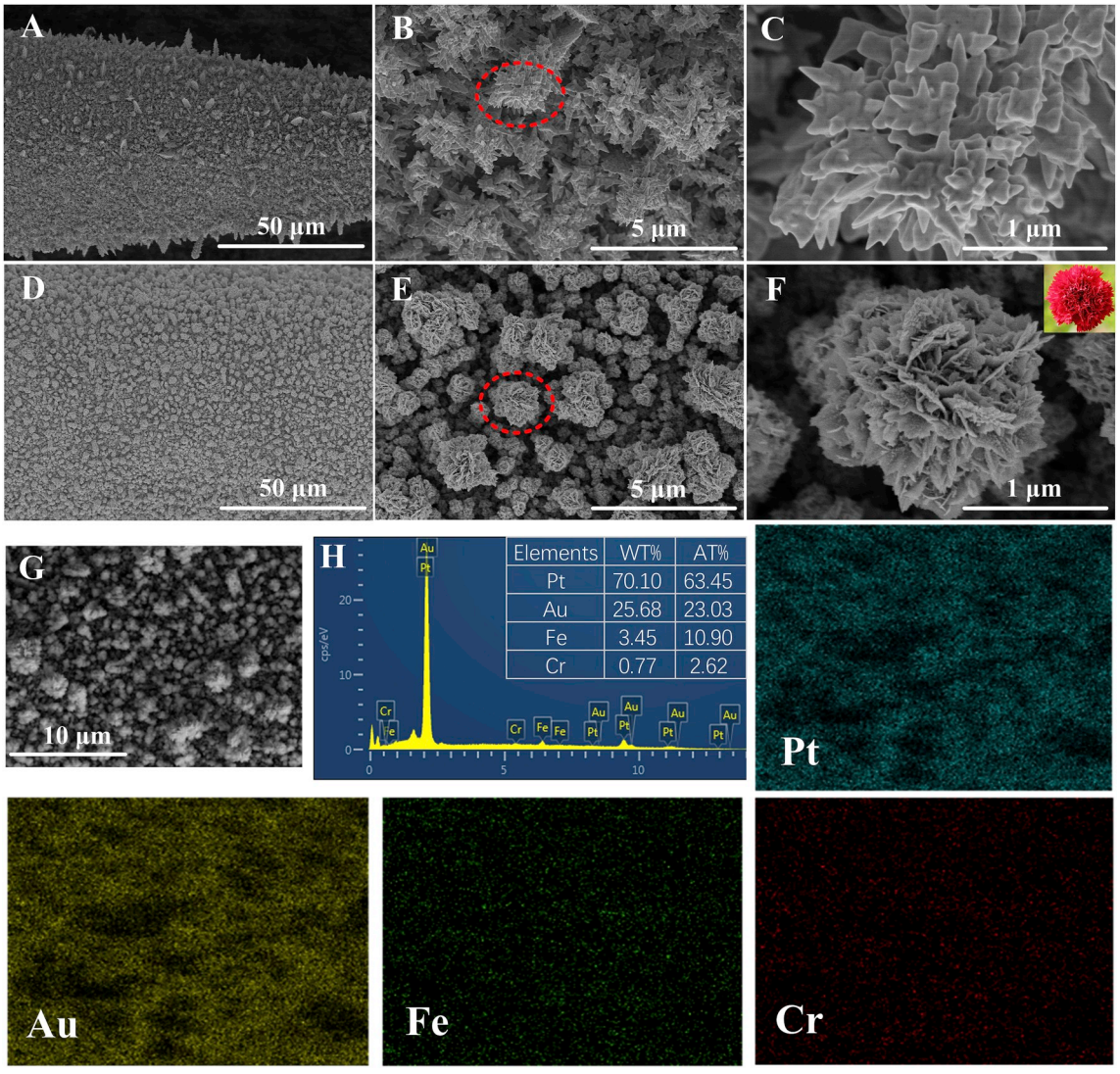

Fig. 1. SEM images of Au spikes (A) (B) (C) and 3D Pt nanoflowers outside the Au spikes (D) (E) (F) at different magnification. (C) and (F) are the high magnification images of the structures in the red circles from (B) and (F). (G) SEM image of electrode surface area for EDS analysis. (H) EDS spectrum and the corresponding elemental mapping images of Pt, Au, Fe and Cr. The inset: the weight ratio and the atomic ratio of Pt, Au, Fe and Cr. (For interpretation of the references to colour in this figure legend, the reader is referred to the Web version of this article.)

platinum deposition observed on the electrode surface covered by hot glue adhesive in subsequent electrochemical deposition experiments, implying that the needle-type microelectrodes have been fabricated successfully through such a simple method. 3D bimetallic Au/Pt nanoflowers modification was integrated onto the needle-type microelectrode and the structure and morphology was characterized by SEM. In Fig. 1A, Au spikes are uniformly decorated on the surface of microelectrode and some small sheets have partly formed. The structure of the red circle in Fig. 1B has been magnified in Fig. 1C with a higher resolution and spike-like morphology can be clearly identified. Afterwards, the surface of microelectrode is covered by spherical particles after platinization outside Au spikes, as shown in Fig. 1D. The high-resolution image of the structure in the red circle in Fig. 1E is displayed in Fig. 1F and a flower-like structure has formed, called Pt nanoflowers. The Pt nanoflowers have a hierarchical carnation-like morphology, which were assembled from hundreds of Pt nanoplates. The average diameter of a single nanoflower is about 1 μm and the average thickness of petals reaches about 25 nm. In addition, there are some smaller spherical particles in Fig. 1E and the high magnification image is shown in Fig. S1. They are also Pt nanoflowers and have a diameter of about 500 nm, but with a hydrangea-like morphology. In fact, these two nanoflowers with different morphologies are at different growth stages of Pt nanoflowers, suggesting a progressive process of nanoflower assembly. At the beginning, Au spikes are electrodeposited on the microelectrode with non-uniform current distribution derived from the spike-like morphology and provide crystal nucleus sites for subsequent Pt growth. Then Pt nanoplates are formed in the vicinity of the electrode and gather to Au spikes, forming the hydrangea-like nanoflowers. When the platinization time extends, Pt nanoplates continue to aggregate and carnation-like nanoflowers are developed. However, the growth rate of Pt nanoflowers depends on local current density, which is inconsistent on the surface of Au spikes. Therefore, carnation-like nanoflowers and hydrangea-like nanoflowers exist at the same time.

EDS spectrums have been recorded to characterize the chemical composition of Au/Pt nanoflowers, revealing the characteristic peaks of metallic Pt, Au, Fe and Cr. Fe and Cr are derived from the substrate, the stainless-steel acupuncture needle. The inset of Fig. 1H displays that the weight ratio of Pt to Au is 70.10:25.68 and the atomic ratio of Pt to Au is 63.45:23.03. EDS elemental mapping measurements were also conducted to characterize the elemental distribution of Au/Pt nanoflowers. Obviously, Au and Pt are both homogeneous distributed, confirming the formation of Au/Pt composites. The distribution zone of Pt (in blue) is almost the same as that of Au (in yellow), manifesting that the Pt nanoflowers were developed right above the Au spikes. Therefore, the structure of Au spikes might have a great influence on the morphology of Pt nanoflowers, which will be explored in follow-up work.

All in all, SEM and EDS analysis have validated the successful growth of Au/Pt nanoflowers. Au spikes are integrated as the base layer and provide a large surface area with non-uniform current distribution for follow-up growth of Pt, developing nanoflower-like morphology and increasing the loading of Pt. The Pt nanoflowers have been electrochemically synthesized with a high surface-to-volume ratio and can provide numerous active sites for enzyme immobilization and redox reactions.

3.2. Electrochemical performance enhancement of 3D bimetallic Au/Pt nanoflowers

In order to explore the electrochemical performance of 3D bimetallic Au/Pt nanoflowers, H_2O_2 tests were conducted to detect the oxidation current at the surface of microelectrodes. Fig. 2A shows the typical current-time response for successive additions of H_2O_2 for bare electrode (in blue), Pt modified electrode (in magenta) and bimetallic Au/Pt nanoflowers modified electrode (in red) at an applied potential of 0.6 V respectively. Fig. 2B displays the corresponding sensitivity comparisons of these electrodes (n = 3). The bare electrode showed a low sensitivity

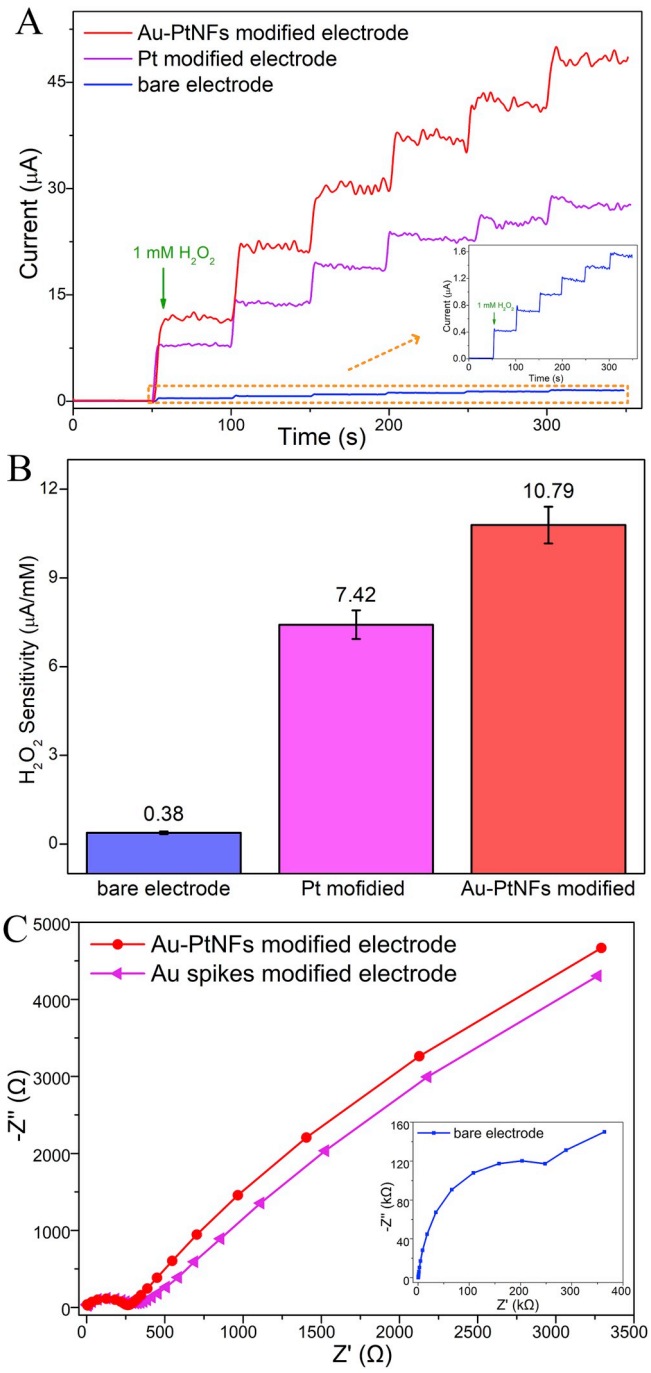

Fig. 2. (A) Typical current-time response for successive additions of H_2O_2 for bare electrode (in blue), Pt modified electrode (in magenta) and bimetallic Au/Pt nanoflowers modified electrode (in red) at an applied potential of 0.6 V. The inset is the magnification of current response of bare electrode. (B) The corresponding sensitivity comparisons of these electrodes (n = 3). (C) EIS spectra of Au/Pt nanoflowers modified electrode (in red) and Au spikes modified electrode (in magenta) in 0.1 M KCl aqueous solution containing 5 mM $K_3[Fe(CN)_6]/K_4[Fe(CN)_6]$. The inset shows full scale of the EIS spectra of bare electrode (in blue). (For interpretation of the references to colour in this figure legend, the reader is referred to the Web version of this article.)

of 0.38 ± 0.05 μA/mM, while the Pt modified electrode had a sensitivity of 7.42 ± 0.48 μA/mM, confirming the electrocatalytic ability of Pt towards H_2O_2. The performance of the electrodes modified with Au spikes only was not shown here due to its bulky structures and low sensitivity towards H_2O_2. The 3D bimetallic Au/Pt nanoflowers modified electrode

provided a markedly improved sensitivity of 10.79 ± 0.62 μA/mM than that of Pt modified electrode. This could be attributed to the enhanced conductivity, a larger electroactive surface area and more active sites with the specific nanoflower-like morphology, resulting from the introduction of Au spikes as the base layer. The synergetic effect of Au and Pt induces a remarkable electrocatalytic activity towards the electrochemical oxidation of H_2O_2: the Au spikes act as the base layer with non-uniform current distribution and enhanced conductivity; the Pt nanoflowers act as the catalytic layer and exhibit a large electroactive surface area.

The electron-transfer property of 3D bimetallic Au/Pt nanoflowers has been examined by EIS and the Nyquist plots are shown in Fig. 2C. The charge transfer resistance (R_{ct}) of the electrode equals to the semicircle diameter. The resistance of Au spikes (300 Ω) modified electrode is much smaller than that of bare electrode (437 kΩ) in the high-frequency domain, indicating that Au spikes dramatically reduced electrode impedance, improved conductivity and electron transfer. When Pt nanoflowers introduced onto Au spikes for its catalytic ability, the resistance of bimetallic Au/Pt nanoflowers further decreased to 240 Ω, due to the enhanced conductivity from Pt, much higher surface area from the nanoflower-like morphology and the synergistic effect of Au and Pt, leading to a faster electron transfer on the electrode surface.

3.3. Electrochemical performance of ATP biosensor

3D bimetallic Au/Pt nanoflowers provided a high sensitivity of 1.13 ± 0.06 mA mM^{-1} cm^{-2} and a low detection limit of 1 μM for H_2O_2 detection after optimization and made it possible to detect ATP at a low concentration. In addition, considering the mechanism of ATP biosensor based on GOx and HEX, the glucose performance of proposed ATP biosensor was assessed to obtain an accurate response of ATP, and a sensitivity of 84.67 ± 4.53 μA mM^{-1} cm^{-2} with a low detection limit of 10 μM were obtained. The details are all demonstrated in Supporting Information.

A typical current response of ATP biosensor based on bimetallic Au/Pt nanoflowers in the presence of 3 mM glucose is demonstrated in Fig. 3A. The reason for choosing 3 mM glucose is shown in Fig. S5. The inset depicts the details of successive ATP additions for low concentration detection and 2.5 μM ATP can be easily detected. Fig. 3B shows the corresponding calibration curve for a series of 3 ATP biosensors with good reproducibility. The decrease of electrochemical current response is proportional to the ATP concentration. The biosensor exhibited a linear dynamic range from 2.5 μM to 447 μM (R^2 = 0.9947), and the detection limit was estimated to be 2.5 μM (S/N = 3). The linear equation is $i = -1.1069\,C - 29.363$ (i in nA, C in μM), with the sensitivity of 1.29 ± 0.11 nA μM^{-1} mm^{-2}. The satisfactory sensitivity may be attributed to the improved catalytic activity and electron transfer capacity caused by the synergic effect.

To assess the long-term stability, a series of 6 ATP biosensors based on bimetallic Au/Pt nanoflowers were stored in PBS at 4 °C for two weeks. Fig. 3C displays the normalized current response for glucose and ATP respectively, which was normalized with that of the first day. There was an obvious current decrease after two days for both ATP and glucose and the current response remained notably stable afterwards. After two

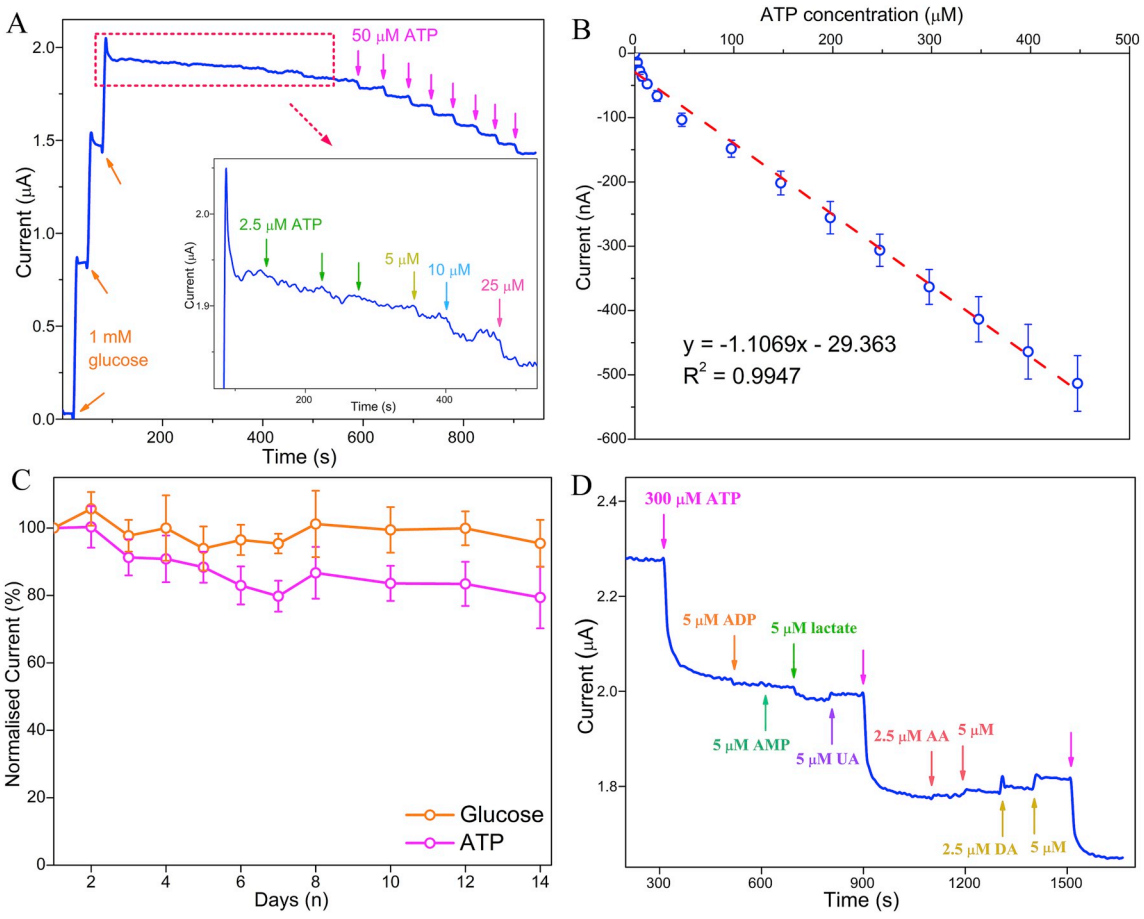

Fig. 3. (A) A typical electrochemical response of ATP biosensor based on Au/Pt nanoflowers in the presence of 3 mM glucose. The inset shows the current response at low ATP concentration. (B) The corresponding calibration curve of ATP biosensor (n = 3). (C) Long-term stability of the ATP biosensor stored in PBS at 4 °C for two weeks (n = 6). Data are shown in the normalized current response for glucose and ATP. (D) Biological interferences test for ATP biosensor at an applied potential of 0.6 V with 300 μM ATP, 5 μM ADP, 5 μM AMP, 5 μM lactate, 5 μM UA, 2.5 μM AA, 5 μM AA, 2.5 μM DA and 5 μM DA.

Table 1
Comparisons of analytical performance of ATP microelectrode biosensors based on glucose oxidase and hexokinase.

Electrodes	Linear range	Stability	Ref.
Pt/GOx-HEX-BSA-glycerol/glutaraldehyde	15–100 μM	−18 °C 50 days, 43% ATP loss, no glucose loss	Kucherenko et al. (2014)
Pt/GOx-HEX-poly phenol	–	7 days, 23.92 ± 3.55% ATP loss, 15.87 ± 1.34% glucose loss,	Patel et al. (2011)
Silica hybrid sol-gel film/GOx-HEX	0.5–20 μM	4 °C 21 days, 40% ATP loss, 20% glucose loss	Liu and Sun (2007)
Pt/GOD-HEX-Canguard polymer	0.2–1 μM	4 °C 14 days, 60% ATP loss, 25% glucose loss	Kueng et al. (2004)
Pt/poly(benzoxazine)-GOx-HEX	0.3–8 μM	4 °C 8 days, 60% ATP loss	Ziller et al. (2017)
Au-PtNFs/GOx-HEX/glutaraldehyde	2.5–447 μM	4 °C 14 days, 20.61 ± 9.15% ATP loss, 4.56 ± 6.97% glucose loss	This work

weeks, the ATP biosensors still maintained 95.44 ± 6.97% of its original response to glucose and 79.39 ± 9.15% of its initial sensitivity to ATP. Fig. S6 shows the glucose and ATP sensitivity changes according to calibration curves. The final sensitivity to glucose is 0.67 ± 0.08 μA mM^{-1} and the final sensitivity to ATP is 1.01 ± 0.09 nA μM^{-1}. Several ATP microelectrode biosensors based on GOx and HEX reported previously have been summarized in Table 1. The superior long-term stability may be due to the enzyme activity preservation by 3D bimetallic Au/Pt nanoflowers, providing a large surface area and enhanced number of active sites, enhancing the adsorption efficiency of enzyme on its petals and maintaining the enzyme activity.

The selectivity of the proposed ATP biosensors against common biological interferences has also been investigated. The concentrations of interferences were chosen from the highest concentrations observed in physiological measurements (Bertrand and Bertrand, 2010; Patel et al., 2011). Fig. 3D demonstrates current response of 300 μM ATP in the presence of adenosine diphosphate (ADP), adenosine monophosphate (AMP), lactate, uric acid (UA), ascorbic acid (AA), dopamine (DA) in 0.01 M PBS at an applied potential of 0.6 V. The current response induced by these biological interferences could be negligible. When 300 μM ATP was added again and again, the current response still decreased even in the presence of these interferences, suggesting a high selectivity of the proposed ATP biosensors.

3.4. Direct in situ determination of ATP secreted from living cells

Due to the superior electrochemical performance of ATP biosensor (e.g. sensitivity, detection limit, selectivity, stability and reproducibility), the 3D bimetallic Au/Pt nanoflowers decorated needle-type microelectrode is able to be used for studying the change of ATP level secreted from living cells as shown in Fig. 4. The PC12 cell line is a useful model for cell signaling or neurosecretion (Vaudry et al., 2002; Westerink and Ewing, 2008) and high K^+ solutions can induce a significant release of ATP from PC12 cells has been reported (Fabbro et al., 2004; Kasai et al., 2001). Fig. 4A displays a typical current-time response curve recorded at the ATP biosensor with PC12 cells (in red) and without PC12 cells (in blue). The background current in the red curve is higher than that of the blue curve, maybe due to the existence of cells. First of all, 2.5 μL blank solution (PBS containing 3 mM glucose and 18 mM magnesium) was added. The current reached the current level before addition after some fluctuations, indicating that the addition action has little effect on the current response. Then a high K^+ solution (2.5 μL 0.1

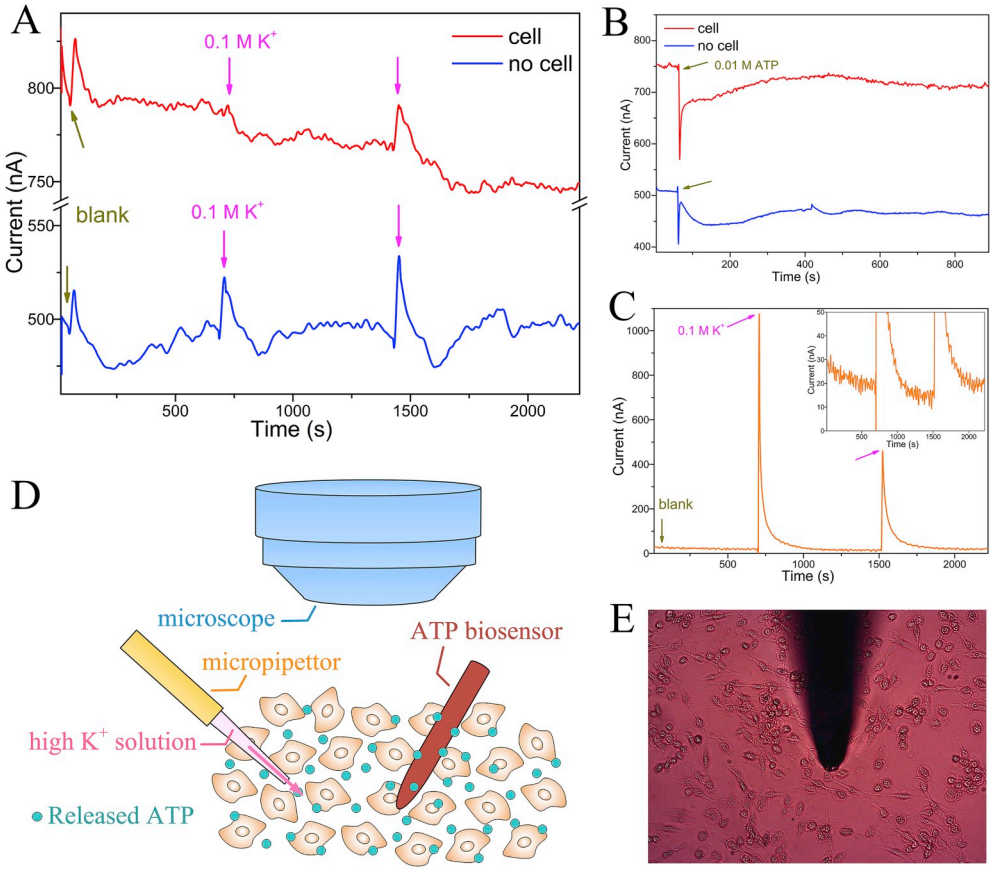

Fig. 4. Local determination of ATP secreted from PC12 cells. (A) Typical current-time response curve recorded at the ATP biosensor with PC12 cells (in red) and without PC12 cells (in blue). (B) Current-time response curve recorded at the ATP biosensor stimulated by external ATP solution with PC12 cells (in red) and without PC12 cells (in blue). (C) Current-time response curve recorded at the bare electrode (only modified with 3D Pt nanoflowers, without enzyme immobilization) with PC12 cells. (D) Schematic illustration of *in situ* detection of cellular ATP release using the micro-needle tip electrode decorated with 3D Pt nanoflowers. (E) Optical microscope photo of microelectrode and cells. (For interpretation of the references to colour in this figure legend, the reader is referred to the Web version of this article.)

M) was added to stimulate cells to release ATP. Remarkable decreases in current response were induced by the addition of K^+ in the experiment with cells, while there was no obvious current decline in the experiment without cells. In all experiments (N = 6), the value of the current drop in each addition of 0.1 M K^+ was about 21.6 ± 3.4 nA, corresponding to 12.2 ± 2.8 μM ATP, as shown in Table S3. As reported previously (Zhang et al., 2016; Ziller et al., 2017), the obtained concentration of ATP released from cells is in the micromolar range. Thus, the determined ATP levels secreted from PC12 cells in this work are consistent with the suggested levels.

To ensure that the ATP biosensors are still effective after detection, external ATP stimulation solution was added afterwards in both experiments, as shown in Fig. 4B. External ATP (2.5 μL 0.01 M) both led to a significant current decrease of about 42 nA, indicating that the ATP biosensors are still at work. In addition, to investigate whether other redox-active biological molecules are co-released and falsify ATP signal during K^+ stimulation or not, a bimetallic Au/Pt nanoflowers decorated needle-type microelectrode without enzymes was used to record the current response in the culture dish with PC12 cells. Fig. 4C displays an exemplary current-time curve with K^+ stimulation. The background current is much lower than that from the red curve in Fig. 4A, because there was no GOx immobilized on this microelectrode so the current generated by glucose oxidation declined. The equilibrium current was around 15–20 nA all the time and no significant current decrease was observed, indicating that no obvious current changes induced by other molecules falsified the ATP signal. Fig. 4D shows the schematic illustration of *in situ* determination of cellular ATP release with the proposed ATP biosensor. ATP is released from cells upon stimulation and directly detected on the microelectrode near the cells. Fig. 4E is the optical microscope photo of microelectrode and cells. The above results indicate that the bimetallic Au/Pt nanoflowers decorated needle-type microelectrode can realize direct *in situ* monitoring of ATP secreted from living cells successfully.

4. Conclusions

In summary, an ATP microelectrode biosensor based on 3D bimetallic Au/Pt nanoflowers by template-free electrodeposition was fabricated and realized local detection of cellular ATP secretion. The needle-type microelectrode was obtained with a simple microelectrode package protocol and layer-by-layer 3D bimetallic Au/Pt nanoflowers were introduced: the Au spikes act as the base layer with non-uniform current distribution and enhanced conductivity; the Pt nanoflowers act as the catalytic layer and exhibit a large electroactive surface area and good compatibility with numerous active sites for enzyme. A dual enzyme ATP biosensor was developed and exhibited a low limit of detection, excellent long-term stability, high selectivity and satisfactory sensitivity. The ATP biosensor was then used for direct *in situ* monitoring of ATP secreted from living cells and several contrast tests are conducted to ensure the validity. The change of ATP levels induced by stimulation of high K^+ solutions was identified successfully and consistent with the suggested levels. The 3D bimetallic Au/Pt nanoflowers possess excellent catalytic activity and large electroactive surface area, contributing to enzymatic activity preservation and long-term stability. The proposed biosensor would be further explored for monitoring the level fluctuation of ATP or other secretions in cellular glycolysis and apoptosis processes in the future.

Declaration of competing interest

The authors declare that they have no known competing financial interests or personal relationships that could have appeared to influence the work reported in this paper.

CRediT authorship contribution statement

Qin Zhu: Conceptualization, Methodology, Visualization, Investigation, Formal analysis, Supervision, Validation, Writing - original draft, Writing - review & editing, Data curation, Resources, Project administration. **Bo Liang:** Funding acquisition, Supervision, Methodology, Validation, Conceptualization, Project administration, Writing - original draft, Writing - review & editing. **Yitao Liang:** Validation, Resources, Formal analysis, Visualization. **Lin Ji:** Resources, Validation. **Yu Cai:** Formal analysis, Investigation, Resources. **Ke Wu:** Investigation. **Tingting Tu:** Investigation, Visualization. **Hangxu Ren:** Investigation. **Bobo Huang:** Methodology. **Jinwei Wei:** Writing - review & editing, Methodology. **Lu Fang:** Conceptualization. **Xiao Liang:** Resources, Investigation. **Xuesong Ye:** Funding acquisition, Conceptualization, Supervision, Writing - review & editing.

Acknowledgment

This work was financially supported by Natural Science Foundation of Zhejiang Province, China (LQ20F010011, LY18H180006); Key Research and Development Program of Zhejiang Province, China (2019C03066); National Natural Science Foundation of China, China (61501400, 81501555).

Appendix A. Supplementary data

Supplementary data to this article can be found online at https://doi.org/10.1016/j.bios.2020.112019.

References

Beigi, R., Kobatake, E., Aizawa, M., Dubyak, G.R., 1999. Am. J. Physiol. Cell Physiol. 276, C267–C278.
Bertrand, P.P., Bertrand, R.L., 2010. Auton. Neurosci. Basic Clin. 153, 47–57.
Burnstock, G., 2016. Philos. Trans. R. Soc. Biol. Sci. 371 (1700).
Burnstock, G., 2007. Physiol. Rev. 87, 659–797.
Chen, Z., Shen, R., Chen, C., Li, J., Li, Y., 2018. Chem. Commun. (Camb) 54, 13155–13158.
D, A.J., Parimaladevi, R., A, A.J.A., Sathe, G.V., Umadevi, M., 2018. Colloids Surfaces A Physicochem. Eng. Asp. 554, 218–226.
Deng, J., Wang, K., Wang, M., Yu, P., Mao, L., 2017. J. Am. Chem. Soc. 139, 5877–5882.
Evans, R.J., Derkach, V., Surprenant, A., 1992. Nature 357, 503–505.
Fabbro, A., Skorinkin, A., Grandolfo, M., Nistri, A., Giniatullin, R., 2004. J. Physiol. 560, 505–517.
Gilroy, K.D., Ruditskiy, A., Peng, H.C., Qin, D., Xia, Y., 2016. Chem. Rev. 116, 10414–10472.
Gourine, A.V., Llaudet, E., Dale, N., Spyer, K.M., 2005. Nature 436, 108–111.
Guo, M.Q., Hong, H.S., Tang, X.N., Fang, H.D., Xu, X.H., 2012. Electrochim. Acta 63, 1–8.
Hecht, E., Liedert, A., Ignatius, A., Mizaikoff, B., Kranz, C., 2013. Biosens. Bioelectron. 44, 27–33.
Kasai, Y., Ohta, T., Nakazato, Y., Ito, S., 2001. J. Vet. Med. Sci. 63, 367–372.
Kucherenko, I.S., Didukh, D.Y., Soldatkin, O.O., Soldatkin, A.P., 2014. Anal. Chem. 86, 5455–5462.
Kueng, A., Kranz, C., Mizaikoff, B., 2004. Biosens. Bioelectron. 19, 1301–1307.
Liu, S., Sun, Y., 2007. Biosens. Bioelectron. 22, 905–911.
Liu, Y., Chen, J., Du, M., Wang, X., Ji, X., He, Z., 2017. Biosens. Bioelectron. 92, 68–73.
Ma, Y., Geng, F., Wang, Y., Xu, M., Shao, C., Qu, P., Zhang, Y., Ye, B., 2019. Biosens. Bioelectron. 134, 36–41.
Morciano, G., Sarti, A.C., Marchi, S., Missiroli, S., Falzoni, S., Raffaghello, L., Pistoia, V., Giorgi, C., Di Virgilio, F., Pinton, P., 2017. Nat. Protoc. 12, 1542–1562.
Oliveira, A.G., Marques, P.E., Amaral, S.S., Quintão, J.L.D., Cogliati, B., Dagli, M.L.Z., Rogiers, V., Vanhaecke, T., Vinken, M., Menezes, G.B., 2013. Liver Int. 33 (3), 353–361.
Patel, B.A., Rogers, M., Wieder, T., O'Hare, D., Boutelle, M.G., 2011. Biosens. Bioelectron. 26, 2890–2896.
Patergnani, S., Baldassari, F., De Marchi, E., Karkucinska-Wieckowska, A., Wieckowski, M.R., Pinton, P., 2014. Methods Enzymol. 313–332.
Qian, Y., Wang, X., Li, Y., Cao, Y., Chen, X., 2016. Mol. Cancer Res. 14, 1087–1096.
Robinson, D.L., Hermans, A., Seipel, A.T., Wightman, R.M., 2008. Chem. Rev. 108 (7), 2554–2584.
Russell, C., Ward, A.C., Vezza, V., Hoskisson, P., Alcorn, D., Steenson, D.P., Corrigan, D. K., 2019. Biosens. Bioelectron. 126, 806–814.
Secundo, F., 2013. Chem. Soc. Rev. 42, 6250–6261.
Tang, S., Shen, H., Hao, Y., Huang, Z., Tao, Y., Peng, Y., Guo, Y., Xie, G., Feng, W., 2018. Biosens. Bioelectron. 104, 72–78.
Taurino, I., Sanzó, G., Mazzei, F., Favero, G., De Micheli, G., Carrara, S., 2015. Sci. Rep. 5, 15277.

Vaudry, D., Stork, P.J.S., Lazarovici, P., Eiden, L.E., 2002. Science 80.
Wang, Z., Zhang, Y., Ju, E., Liu, Z., Cao, F., Chen, Z., Ren, J., Qu, X., 2018. Nat. Commun. 9, 3334.
Westerink, R.H.S., Ewing, A.G., 2008. Acta Physiol. 273–285.
Yang, N.C., Ho, W.M., Chen, Y.H., Hu, M.L., 2002. Anal. Biochem. 306, 323–327.
Yang, Z., Liu, X., Zheng, X., Zheng, J., 2018. J. Electroanal. Chem. 817, 48–54.
Yao, W., Wang, L., Wang, H., Zhang, X., Li, L., 2009. Biosens. Bioelectron. 24, 3269–3274.
Zhang, Y., Clausmeyer, J., Babakinejad, B., López Córdoba, A., Ali, T., Shevchuk, A., Takahashi, Y., Novak, P., Edwards, C., Lab, M., Gopal, S., Chiappini, C., Anand, U., Magnani, L., Coombes, R.C., Gorelik, J., Matsue, T., Schuhmann, W., Klenerman, D., Sviderskaya, E.V., Korchev, Y., 2016. ACS Nano 10, 3214–3221.
Zhang, Z., Chen, G., Zhou, W., Song, A., Xu, T., Luo, Q., Wang, W., Gu, X.S., Duan, S., 2007. Nat. Cell Biol. 9, 945–953.
Ziller, C., Lin, J., Knittel, P., Friedrich, L., Andronescu, C., Pöller, S., Schuhmann, W., Kranz, C., 2017. ChemElectroChem 4, 864–871.